

Precision Data-enabled Koopman-type Inverse Operators for Linear Systems [★]

Leon (Liangwu) Yan ^{*} Santosh Devasia ^{**}

^{*} *Mechanical Engineering Department, University of Washington, Seattle, WA 98195-2600, USA (e-mail: liangy00@uw.edu).*

^{**} *Mechanical Engineering Department, University of Washington, Seattle, WA 98195-2600, USA (e-mail: sdevasia@uw.edu)*

Abstract: The advent of easy access to large amount of data has sparked interest in directly developing the relationships between input and output of dynamic systems. A challenge is that in addition to the applied input and the measured output, the dynamics can also depend on hidden states that are not directly measured. The main contribution of this work is to identify the information needed (in particular, the past history of the output) to remove the hidden state dependence in Koopman-type inverse operators for linear systems. Additionally, it is shown that the time history of the output should be augmented with the instantaneous time derivatives of the output to achieve precision of the inverse operator. This insight into the required output (history and instantaneous derivative) information, to remove the hidden-state dependence and improve the precision of data-enabled inverse operators, is illustrated with an example system.

Keywords: Dynamics, hidden state dependency, neural-network models, inverse models

1. INTRODUCTION

With increasing ease of collecting data and low cost storage, there is increasing interest to use data-enabled methods developing models for prediction and control, Abraham et al. (2017); Mamakoukas et al. (2021); Hewing et al. (2020); Asadi et al. (2021); Piche et al. (2000); Kabzan et al. (2019); Kocijan et al. (2004). Such models can be optimized to best fit the data and methods are also available to estimate the error bounds on the predictions, e.g., using predicted time derivatives of the observables Mamakoukas et al. (2021). However, the conditions under which such data-enabled models can achieve sufficient precision remains unclear. A major challenge is that the model (i.e., the relationship between the input and the measurable outputs) can be dependent on the system's internal states, which are hidden in the sense that they are not directly measured, nor inferred using standard observer designs since they require prior knowledge of the system dynamics.

Several approaches are available to address the lack of direct access to the hidden states. One approach is to represent the dynamics through Markov models with a predefined number of hidden states, and then minimize the model prediction error Tarbouriech et al. (2020); Yoon et al. (2019); Pohle et al. (2017). A difficulty is that the optimal selection of the number of hidden states can be computationally expensive, and there is no guarantee that the resulting models will achieve the desired precision. A second class of approaches to handle the lack of direct access to the hidden states is to model the system dynamics (flow) in a lifted observable space (with generalized functions of the observables) using Koopman operator theory Schmid and Sesterhenn (2008); Mezić (2005). Re-

cent techniques include sparse identification of nonlinear dynamical systems (SINDy) Brunton et al. (2016) and linearization Dynamic Mode Decomposition(DMD) Kutz et al. (2016). Nevertheless, with a finite number of states, there is uncertainty about how to select a sufficient set of generalized observable functions to achieve a specified level of prediction precision. A third class of approaches is to use time history of the input and output data to find forward models, e.g., with (i) transfer function models in the frequency domain Devasia (2017); Yan et al. (2021); (ii) autoregressive models with extra input (ARX) Ljung et al. (1987) as well as nonlinear ARX (NARX) Kocijan et al. (2004); Pham et al. (2010); (iii) time-delayed information in the Koopman operator framework Kamb et al. (2020); and fitting a relation between the time-delayed output data and the inverse input Butterworth et al. (2012); Blanken and Oomen (2020); Aarnoudse et al. (2021). Again, determining the type of data needed to capture the input-output relationship (with high precision) when models are not available a-priori remains uncertain. When precision of the inverse is not sufficient, it can be improved using iterative techniques, with the inverse of the plant considered as the learning operator, Ghosh and Paden (2001); Fine et al. (2009); Teng and Tsao (2015); Spiegel et al. (2021). Nevertheless, increasing the precision of the inverse model can improve ILC convergence.

The goal of this article is to identify the type of output data needed to develop inverse (output-to-input) operators, with a desired level of precision. Rather than the two step processes of first learning forward models and second using model-predictive control (MPC) to optimally select the control input, the proposed approach seeks to solve the inverse problem of directly finding the input for a given output, e.g., similar to Devasia et al. (1996); Willems et al.

[★] This work was supported by NSF Grant CMMI 1824660.

(2005). In particular, the relative degree of the system is used to identify the number of time derivatives that need to be added to input-output data to facilitate precision data-enabled learning of the inverse operator.

Previous works on inversion of system dynamics, using known models of the system, have shown that the impact of neglecting the boundary conditions of the internal states can be made arbitrarily small Zou and Devasia (1999, 2007) by choosing a sufficiently large time history of the desired output and its derivatives. This motivates the proposed data-enabled algorithm to learn the inverse operator directly from input-output data (without the need to explicitly capture the hidden state dynamics) by using time-delayed observations of the output, along with the output's time derivatives.

The main contribution of this paper is to propose a Koopman-type time-delay and output-derivative-based data-enabled inverse operator that minimizes the impact of the hidden state dependency and achieves precision (illustrated with a simulation example). Overall, the work provides insight into the need for including derivative features and time history to achieve precision in Koopman-type inverse operators. Even for forward Koopman-type operators (which only depend on past observable outputs) it is shown that the output-derivative at the current time instant needs to be included for precision prediction.

2. PROBLEM FORMULATION AND SOLUTION

The inverse operator is developed for linear time-invariant (LTI) single-input-single-output (SISO) system. Let the system be

$$\dot{x}(t) = Ax(t) + Bu(t) \quad (1)$$

$$y(t) = Cx(t) \quad (2)$$

with states $x(t) \in \mathbb{R}^n$, input $u(t) \in \mathbb{R}$ and output $y(t) \in \mathbb{R}$ with matrices $A \in \mathbb{R}^n \times \mathbb{R}^n$, $B \in \mathbb{R}^n \times 1$, $C \in 1 \times \mathbb{R}^n$.

Assumption 1. (System properties). The system described in (1) and (2) is stable (i.e., A is Hurwitz), hyperbolic (no zeros on the imaginary axis), and has relative degree $r \leq n$ (i.e., the difference between the number of poles and the number of zeros).

Assumption 2. The desired output y_d , specified in inverse operator problems, is sufficiently smooth, and has bounded time derivatives up to the relative degree r .

2.1 Hidden state dependency

The system state x can split into state components ξ that directly depend on the output and its time derivatives

$$\xi(t) = [y(t), \dot{y}(t), \dots, \frac{d^{r-1}y(t)}{dt^{r-1}}]' \in \mathbb{R}^{r \times 1} \quad (3)$$

and internal states η ,

$$\begin{bmatrix} \xi(t) \\ \eta(t) \end{bmatrix} = Sx(t) \quad (4)$$

such that in the new coordinates, (1) can be written as, e.g., see Marino and Tomei (1995), Example 4.1.3,

$$\dot{\xi}(t) = A_1\xi(t) + A_2\eta(t) + B_1u(t) \quad (5)$$

$$\dot{\eta}(t) = A_3y(t) + A_4\eta(t) \quad (6)$$

where

$$B_1 = \begin{bmatrix} 0 \\ 0 \\ \vdots \\ b_{n-r} \end{bmatrix} \in \mathbb{R}^{r \times 1}, \quad A_3 = \begin{bmatrix} 0 \\ 0 \\ \vdots \\ 1/b_{n-r} \end{bmatrix},$$

$$A_4 = \begin{bmatrix} 0 & 1 & \dots & 0 \\ \vdots & \vdots & \ddots & \vdots \\ 0 & 0 & \dots & 1 \\ -b_0/b_{n-r} & -b_1/b_{n-r} & \dots & -b_{n-r-1}/b_{n-r} \end{bmatrix}$$

and the eigenvalues of matrix A_4 are the zeros of the transfer function of system (1) and (2).

$$G(s) = \frac{Y(s)}{U(s)} = \frac{b_0 + b_1s + \dots + b_{n-r}s^{n-r}}{a_0 + a_1s + \dots + a_{n-1}s^{n-1} + s^n}. \quad (7)$$

Note that the internal state η is only driven by the output $y = \xi_1$. Moreover, due to the relative degree r assumption, the input u is directly related to the r^{th} derivative of the output, and therefore, the r^{th} row of (5) can be written as

$$\begin{aligned} y^{(r)}(t) &\triangleq \frac{d^r y(t)}{dt^r} = CA^r x + CA^{r-1}Bu(t) \\ &= CA^r S^{-1} \begin{bmatrix} \xi(t) \\ \eta(t) \end{bmatrix} + b_{n-r}u(t) \\ &= A_\xi \xi(t) + A_\eta \eta(t) + b_{n-r}u(t), \end{aligned} \quad (8)$$

and the matrices A_1 and A_2 in (5) are given by

$$A_1 = \begin{bmatrix} 0 & 1 & \dots & 0 \\ \vdots & \vdots & \ddots & \vdots \\ 0 & 0 & \dots & 1 \\ A_\xi \end{bmatrix}, \quad A_2 = \begin{bmatrix} 0 & 0 & \dots & 0 \\ \vdots & \vdots & \ddots & \vdots \\ 0 & 0 & \dots & 0 \\ A_\eta \end{bmatrix}.$$

where A_ξ and A_η are the last rows of matrices A_1 and A_2 respectively.

2.2 Research problem

The desired output and its derivatives, $(y_d^{(r)}, \xi_d)$ can be used to predict the inverse input u_d from (8), as

$$u_d(t) = b_{n-r}^{-1} [y_d^{(r)}(t) - A_\xi \xi_d(t) - A_\eta \eta_d(t)], \quad (9)$$

which depends on the internal states η that are hidden or not directly measured. The goal is to minimize the hidden state effects on the inverse model, by addressing the following research problems.

- (i) Finding the hidden state from output: Develop an operator that maps the time history of the output y with length T to an estimate of the hidden state η at time t

$$\hat{\eta}(t) = \hat{\mathbb{H}}[y(t-T:t)]. \quad (10)$$

- (ii) Koopman-type inverse operator: Using the operator in (10), develop a data-enabled Koopman-type inverse operator $\hat{\mathbb{G}}^{-1}$ that uses the history of the desired output and its time derivatives to predict the inverse input as

$$\hat{u}_d(t) = \hat{\mathbb{G}}^{-1}[y_d(t-T:t), \xi_d(t), y_d^{(r)}(t)]. \quad (11)$$

- (iii) Inverse operator precision: Quantify the error $\|\hat{u}_d(t) - u_d(t)\|_2$ dependence on each argument of $\hat{\mathbb{G}}^{-1}$.

2.3 Solution

Finding the hidden state from output If the system is minimum-phase (A_4 is Hurwitz), i.e., (7) has no zeros on

the right half plane, then $\eta(t)$ can be obtained from the history of the output by solving (6)

$$\eta(t) = \int_{-\infty}^t e^{A_4(t-\tau)} A_3 y(\tau) d\tau \quad (12)$$

$$\triangleq \mathbb{H}[y(-\infty : t)].$$

In practice, such an operator is hard to capture in a data-enabled way since it requires an infinite window. Therefore, an estimate $\hat{\eta}$ is obtained with an approximate operator $\hat{\mathbb{H}}$ with a finite time history length T is defined

$$\hat{\eta}(t) \triangleq \int_{t-T}^t e^{A_4(t-\tau)} A_3 y(\tau) d\tau \quad (13)$$

$$\triangleq \hat{\mathbb{H}}[y(t-T : t)].$$

The approximate operator $\hat{\mathbb{H}}$ approaches the exact operator \mathbb{H} exponentially as the time history T increases.

Lemma 1. If the output trajectory is bounded,

$$M = \max_{\tau \in [-\infty, t-T]} \|y(\tau)\|_2 < \infty, \quad (14)$$

then the error in computing the hidden state $\eta(t)$ decays exponentially with the time history T , i.e., there exists positive scalars $\alpha_1 > 0, \beta_1 > 0$ such that

$$\|\Delta\eta(t)\|_2 \triangleq \|\eta(t) - \hat{\eta}(t)\|_2 \leq \beta_1 e^{-\alpha_1 T}. \quad (15)$$

Proof. Since the system is assumed to be minimum phase, the and the eigenvalues of matrix A_4 , which are the zeros of the transfer function of system (1), lie in the open left-half of the complex plane, i.e., the matrix A_4 is Hurwitz. Then, there exists positive scalars $\kappa_1 > 0, \alpha_1 > 0$ such that, Desoer and Vidyasagar (1975)

$$\|e^{A_4 t}\|_2 \leq \kappa_1 e^{-\alpha_1 t}. \quad (16)$$

Then, from (12,13), the approximation error can be bounded as

$$\begin{aligned} \|\eta(t) - \hat{\eta}(t)\|_2 &= \left\| \int_{-\infty}^{t-T} e^{A_4(t-\tau)} A_3 y(\tau) d\tau \right\|_2 \\ &\leq M \|A_3\|_2 \int_{-\infty}^{t-T} \kappa_1 e^{-\alpha_1(t-\tau)} d\tau \\ &\quad \text{using (14, 16)} \\ &= M \|A_3\|_2 \int_T^{+\infty} \kappa_1 e^{-\alpha_1 \tau'} d\tau' \\ &= M \|A_3\|_2 \frac{\kappa_1}{\alpha_1} e^{-\alpha_1 T}. \end{aligned} \quad (17)$$

The result follows with

$$\beta_1 = M \|A_3\|_2 \frac{\kappa_1}{\alpha_1}. \quad (18)$$

Koopman-type inverse operator Given an estimate $\hat{\eta}$ of the internal state η , the inverse operator prediction in (11) can be estimated as

$$\begin{aligned} \hat{u}_d(t) &= b_{n-r}^{-1} \left[y_d^{(r)}(t) - A_\xi \xi_d(t) - A_\eta \hat{\eta}_d(t) \right] \\ &= b_{n-r}^{-1} \left[y_d^{(r)}(t) - A_\xi \xi_d(t) - A_\eta \hat{\mathbb{H}}[y_d(t-T : t)] \right] \\ &\quad \text{using (13)} \\ &\triangleq \hat{\mathbb{G}}^{-1}[y_d^{(r)}(t), \xi_d(t), y_d(t-T : t)]. \end{aligned} \quad (19)$$

Remark 1. In addition to sufficient time history (large T) of the output to accurately find the internal state (to let $\Delta\eta \rightarrow 0$), information about the derivatives of the output (upto the relative degree r at time t , i.e., $y_d^{(r)}(t), \xi(t)$) are also needed for precisely computing the inverse input u_d in (11) as illustrated in Fig. 1.

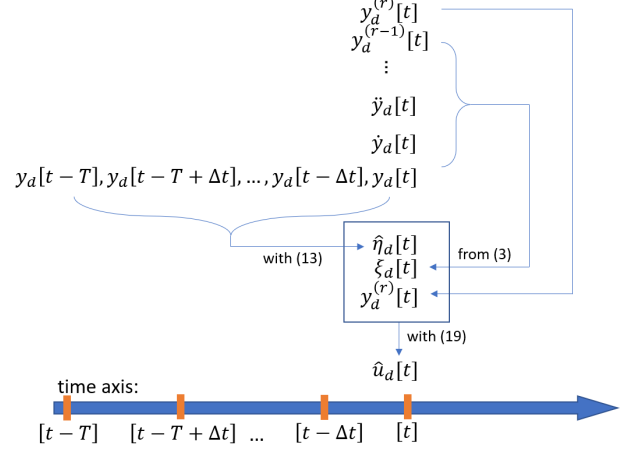


Fig. 1. The inverse operator's dependence on the hidden state is removed by use of past output history and current time derivatives of the output.

Koopman-type forward operators using output history

The output y can be related to the input as

$$y(t+T_f) = C \int_{-\infty}^{t+T_f} e^{A(t-\tau)} B u(\tau) d\tau \quad (20)$$

and approximated by

$$\hat{y}(t+T_f) = C \int_{t-T}^{t+T_f} e^{A(t-\tau)} B u(\tau) d\tau. \quad (21)$$

Therefore, using arguments similar to the proof of Lemma 1, the error in computing the output using just the history of input u tends to zero as the time history of the input increases, i.e., as $T \rightarrow \infty$. Thus, it is possible to find a map that only depends on the input and its past history,

$$\hat{y}(t+T_f) = \hat{\mathbb{G}}_u[u(t-T : t+T_f)], \quad (22)$$

which justifies the use of ARX models to capture forward linear system models using past input history (and augmented by the output history). In contrast, with Koopman-type operators where past history of the observable output is used to predict future values, the forward model prediction can be written as

$$\begin{aligned} \hat{y}(t+T_f) &= C e^{AT_f} \hat{x}(t) + C \int_t^{t+T_f} e^{A(t+T_f-\tau)} B u(\tau) d\tau \\ &= C e^{AT_f} S^{-1} \begin{bmatrix} \xi(t) \\ \hat{\eta}(t) \end{bmatrix} + C \int_t^{t+T_f} e^{A(t+T_f-\tau)} B u(\tau) d\tau \\ &\quad \text{using (4)} \\ &= C e^{AT_f} S^{-1} \begin{bmatrix} \xi(t) \\ \hat{\mathbb{H}}[y_d(t-T : t)](t) \end{bmatrix} \\ &\quad + C \int_t^{t+T_f} e^{A(t+T_f-\tau)} B u(\tau) d\tau \\ &\quad \text{using (13)} \\ &\triangleq \hat{\mathbb{G}}[y(t-T : t), \xi(t), u(t : t+T_f)]. \end{aligned} \quad (23)$$

Therefore, past history of the output can also be used to develop Koopman-type forward operators, provided access is available to current time derivatives of the output $\xi(t)$.

Inverse operator precision The inverse operator depends not only on the past history of the output (to remove the hidden state η dependency) but also on the output and its time derivatives at the current time instant t . The impact of the time history T , output and its time derivatives on the precision of the operator is quantified in the next lemma.

Lemma 2. The prediction error of the inverse operator is bounded, i.e there exists positive scalars $L_1 > 0, L_2 > 0, L_3 > 0$ such that the error between the predicted input $\hat{u}_d(t)$ and the true input $u_d(t)$ is

$$\begin{aligned} & \|\hat{u}_d(t) - u_d(t)\|_2 \\ & \leq L_1 \|\Delta y_d^{(r)}(t)\|_2 + L_2 \|\Delta \xi_d(t)\|_2 + L_3 e^{-\alpha_1 T}. \end{aligned} \quad (24)$$

Proof. From (9) and (19),

$$\begin{aligned} & \|\hat{u}_d(t) - u_d(t)\|_2 \\ & \leq |b_{n-r}^{-1}| \left[\|\Delta y_d^{(r)}(t)\|_2 + \|A_\xi\|_2 \|\Delta \xi_d(t)\|_2 \right. \\ & \quad \left. + \|A_\eta\|_2 \|\Delta \eta_d(t)\|_2 \right], \end{aligned} \quad (25)$$

where $\Delta y_d^{(r)}(t) \triangleq \hat{y}_d^{(r)}(t) - y_d^{(r)}(t)$, $\Delta \xi_d(t) \triangleq \hat{\xi}_d(t) - \xi_d(t)$ and $\Delta \eta_d(t) \triangleq \hat{\eta}_d(t) - \eta_d(t)$. The results follows from (15) with

$$L_1 = |b_{n-r}^{-1}|, \quad L_2 = L_1 \|A_\xi\|_2, \quad L_3 = L_1 \|A_\eta\|_2 \beta_1. \quad (26)$$

Remark 2. (Data-enabled algorithm). Known values of the desired output and its derivatives, specified with a sampling period Δt and time history T can be used to estimate a discrete-time inverse operator from (19) as

$$\hat{u}_d[m] = \mathbb{G}_d^{-1}[y_d[m - m_T : 1 : m], \xi_d[m], y_d^{(r)}[m]], \quad (27)$$

where $[m]$ indicates value at time $t_m = m\Delta t$, and $m_T = T/\Delta t$. Data-enabled algorithms can be used to learn the operator \mathbb{G}_d^{-1} , since (27) maps a finite number of variables (desired output and its time derivatives) to the inverse input at time t_m .

3. SIMULATION RESULTS

In this section, an example system is introduced, followed by the data-enabled learning of the inverse operator.

3.1 Example system

Consider the following two-mass-spring-damper system, where the input u is the force acting on mass m_2 and its displacement x_2 is the output y , as shown in Fig. 2.

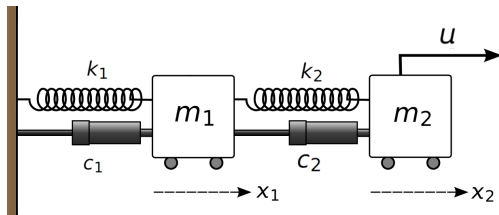


Fig. 2. Example system plot

The corresponding state space model can be written as

$$\frac{d}{dt} X = AX + Bu \quad (28)$$

$$y = x_2 = CX \quad (29)$$

where $X \triangleq [x_1 \dot{x}_1 x_2 \dot{x}_2]^T$, $C = [0 \ 0 \ 1 \ 0]$,

$$A = \begin{bmatrix} 0 & 1 & 0 & 0 \\ -\frac{k_1+k_2}{m_1} & -\frac{c_1+c_2}{m_1} & \frac{k_2}{m_1} & \frac{c_2}{m_1} \\ 0 & 0 & 0 & 1 \\ \frac{k_2}{m_2} & \frac{c_2}{m_2} & -\frac{k_2}{m_2} & -\frac{c_2}{m_2} \end{bmatrix}, \quad B = \begin{bmatrix} 0 \\ 0 \\ 0 \\ a/m_2 \end{bmatrix}, \quad (30)$$

$m_1 = 10, m_2 = 5, k_1 = 110, c_1 = 68, a = k_1/2, k_2 = 75$ and $c_2 = 60$ in SI units. The relative degree of the system is $r = 2$ and the input-output relation is given by

$$\ddot{y}(t) = -25y(t) - 12\dot{y}(t) + 25x_1(t) + 12\dot{x}_1(t) + 11u(t). \quad (31)$$

3.2 Preliminary selections

Selection of the data-enabled model types to evaluate, the sampling time (which needs to be sufficiently small to reduce discretization error), the evaluation metric, and sufficiently smooth output trajectories for model evaluation are described below.

- (i) A two-layer feedforward neural-net (created through MATLAB function `feedforwardnet()` with default activation function) is used to learn the inverse operator from data.
- (ii) For the two-layer neural-net, each model pool consists of 5 candidates with different number $N \in \{5, 10, 20, 40, 80\}$ of neurons in the hidden layer
- (iii) The sampling frequency is varied from 5 Hz to 20 Hz, which is substantially higher than the system bandwidth of 1.7 Hz.

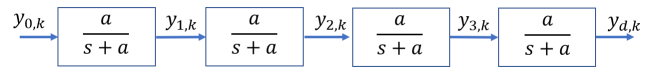


Fig. 3. Filter process to generate desired trajectories.

- (iv) The inverse operator is assessed using 10 different desired trajectories $y_{d,k}(t), 1 \leq k \leq 10, t \in [0, 10]$ with a fixed prediction sampling time of 0.01 s. Each desired trajectory $y_{d,k}$ used for assessment needs to be sufficiently smooth to investigate the impact of different order of output's time derivatives on the inverse operator, although from (24) the expectation is that only output derivatives upto the r^{th} order ($r = 2$ for this example) are required. Therefore, nominal trajectories $y_{0,k}$ (specified in the appendix) are filtered as shown in Fig. 3, to obtain desired outputs $y_{d,k}$ and their derivatives as

$$\begin{bmatrix} y_{d,k} \\ \dot{y}_{d,k} \\ \ddot{y}_{d,k} \\ y_{d,k}^{(3)} \\ y_{d,k}^{(4)} \end{bmatrix} (t) = \begin{bmatrix} 1 & 0 & 0 & 0 & 0 \\ -a & a & 0 & 0 & 0 \\ a^2 & -2a^2 & a^2 & 0 & 0 \\ -a^3 & 3a^3 & -3a^3 & a^3 & 0 \\ a^4 & -4a^4 & 6a^4 & -4a^4 & a^4 \end{bmatrix} \begin{bmatrix} y_{d,k} \\ y_{3,k} \\ y_{2,k} \\ y_{1,k} \\ y_{0,k} \end{bmatrix} (t) \quad (32)$$

where $a = 2\pi$ (cut-off frequency as 1 Hz), which is less than the system's bandwidth of 1.7 Hz, and example trajectories are shown in Fig. 4.

- (v) For a given time history T and sampling time Δt , as in Remark 2, the evaluation metrics for the data-enabled inverse operator with N neurons in the hidden layer are selected as the mean $e_{u,N}$ and maximum $\bar{e}_{u,N}$ normalized prediction error over the ten evaluation trajectories $y_{d,k}(\cdot)$, i.e.,

$$e_{u,N} = \frac{1}{10} \sum_{k=1}^{10} \frac{\max_m |\hat{u}_k[m] - u_{d,k}[m]|}{\max_m |u_{d,k}[m]|} \times 100\% \quad (33)$$

$$\bar{e}_{u,N} = \max_{k=1,\dots,10} \frac{\max_m |\hat{u}_k[m] - u_{d,k}[m]|}{\max_m |u_{d,k}[m]|} \times 100\%, \quad (34)$$

where the ideal inverse $u_{d,k}$ was found using (9) where η_d was obtained through (12). Moreover, the smallest normalized prediction error over different number of neurons in the hidden layer is defined as

$$e_u = e_{u,N^*}, \quad \bar{e}_u = \bar{e}_{u,N^*} \quad \text{where} \quad N^* = \arg \min_N e_{u,N} \quad (35)$$

to quantify the precision of the inverse operator.

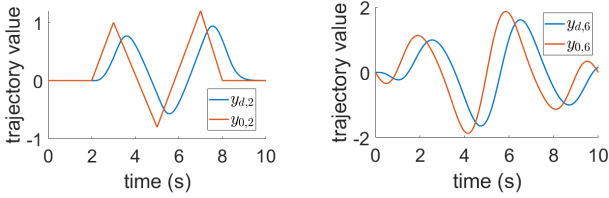


Fig. 4. Comparison of the example filtered desired output $y_{d,k}$ and nominal trajectories $y_{0,k}$ for $k=2$ (triangular) and $k=6$ (sinusoidal).

3.3 Data Collection

The inverse operators are trained using input-output data collected from simulations. Both noisy and noise free output data are used to assess the impact of noise. The input signal u applied to the system is constructed by concatenating 20 cycles of $p_{(f_i, \alpha_i)}(\cdot)$ ($i = 1, 2, 3, \dots, 20$) with different parameters, which are tabulated in Table 1.

$$p_{(f_i, \alpha_i)}(t) = \alpha_i [4 \sin(\pi c t^2) + s(t) + r(t)] \quad (36)$$

where $c = f_i/10$,

$$s(t) = \begin{cases} 1 & 2 \leq t < 4 \\ -0.9 & 4 \leq t < 6 \\ 0.5 & 6 \leq t < 8 \\ 0 & \text{otherwise,} \end{cases} \quad r(t) = \begin{cases} 0.4t & 0 \leq t < 1 \\ 0.4 & 1 \leq t < 9 \\ r(10-t) & 9 \leq t \leq 10. \end{cases}$$

Table 1. Parameters of $p_{(f_i, \alpha_i)}$ in Eq. (36).

Cycle #, i	f_i	α_i	Cycle #, i	f_i	α_i
1	6	0.75	11	1	0.25
2	3	0.5	12	0.5	0.25
3	2	0.5	13	1	-0.1
4	0.5	0.5	14	0.5	-0.05
5	0.5	0.3	15	0.5	0.1
6	0.3	0.3	16	0.5	-0.1
7	0.1	0.3	17	2	0.25
8	0.5	-0.3	18	1	0.1
9	0.3	-0.3	19	0.5	0.05
10	0.1	-0.3	20	1	0.5

For the noisy case, additive white gaussian noise with signal-to-noise ratio of 20 is separately added to each output and its time derivatives. Simulations were done

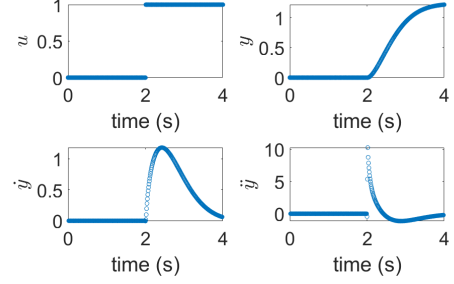


Fig. 5. Identifying the relative degree r from input-output data, based on discontinuity in the r^{th} derivative of the output for a step input.

in MATLAB with `ode45()` with sampling rate of 100 Hz (to be consistent with the evaluation metrics from (33) to (35)). Input, output and the output's time derivatives (upto the fourth order) were collected. Second order derivative was obtained from (31). Third and fourth order derivatives for training purposes were estimated from the data, using finite difference as,

$$\begin{bmatrix} y^{(3)}[m] \\ y^{(4)}[m] \end{bmatrix} = \frac{1}{12(\Delta t)} \begin{bmatrix} -1 & 8 & 0 & -8 & 1 \\ -\frac{1}{\Delta t} & \frac{16}{\Delta t} & -\frac{30}{\Delta t} & \frac{16}{\Delta t} & -\frac{1}{\Delta t} \end{bmatrix} \begin{bmatrix} \dot{y}[m+2] \\ \dot{y}[m+1] \\ \dot{y}[m] \\ \dot{y}[m-1] \\ \dot{y}[m-2] \end{bmatrix}.$$

3.4 Reducing impact of hidden states using output history

To investigate the reduction of the impact of the hidden states on the prediction precision of data-enabled inverse operators, the performance of the data-enabled inverse operators was assessed for different time history T of the output. In this part of the study, the number of time derivatives of the output used was the same as the relative degree of the example system. The relative degree $r=2$ can be established by applying a step input — a corresponding discontinuity will appear in $y^{(r)}$, while the lower order derivatives (y, \dot{y} in this example) remain continuous as seen in Fig. 5. Then, from (27),

$$\hat{u}_d[m] = \mathbb{G}_d^{-1}[y_d[m-m_T : 1 : m], \dot{y}_d[m], \ddot{y}_d[m]]. \quad (37)$$

The inverse operator's prediction error e_u (35) was obtained for varying output time history T ($[0.1, 0.2, 0.4, 0.8, 1.6, 3.2, \dots]$ s), for different sampling time $\Delta t \in \{0.05s, 0.1s, 0.2s\}$, and for different number N of neurons in the hidden layer, and plotted in Fig. 6 for the case without noise in the training data. The associated prediction errors are tabulated in Table 2 for the fastest sampling time $\Delta t = 0.05$ s.

The precision of the inverse operator improves with larger output time history T , as seen in Table 2, where the evaluation values of the two-layer neural net with different N neurons in the hidden layer are listed. Note that typically $N^* \leq 20$ yields good precision for this application from Table 2. Over all selections of neuron numbers N , the variation of the smallest prediction error $e_u = e_{u,N^*}$ (35) with sampling time of $\Delta t = 0.05$ s (20 Hz) fits an exponential decay curve $e_u(T) \approx 1.88e^{-2.18T}$, shown in red in Fig. 6. This exponential improvement in precision is expected from Lemma 2, which predicts an exponential

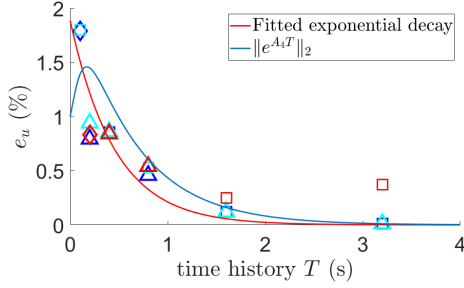


Fig. 6. Inverse operator’s precision in terms of prediction error e_u (35) exponentially improves with respect to different window length T of output history, for different sampling times, $\Delta t = 0.05s$ (20Hz, blue), $0.1s$ (10Hz, cyan), $0.2s$ (5Hz, red). Similar results are seen over different N^* neurons in the hidden layer: 5 triangle (Δ), 10 (square \square), 20 (diamond \diamond), 40 (pentagram \star), and 80 (circle \circ). The fitted exponential decay (red line) is obtained with sampling time of $\Delta t = 0.05$ s (20 Hz, blue).

Table 2. Inverse operator’s precision improvement in terms of prediction error $e_{u,N}$ (33) and $\bar{e}_{u,N}$ (34) for varying output time history T and number N of neurons in the hidden layer, with sampling time $\Delta t = 0.05$ s.

T \ N	5	10	20	40	80
$e_{u,N}(\%)$ as in (33)					
0.1	1.78	2.23	1.64	2.05	2.43
0.2	0.79	0.88	0.87	0.88	0.98
0.4	0.95	0.85	0.88	0.92	0.91
0.8	0.46	0.51	0.49	0.48	0.52
1.6	0.14	0.12	0.12	0.14	0.16
3.2	0.05	0.01	0.01	0.01	0.05
$\bar{e}_{u,N}(\%)$ as in (34)					
0.1	3.17	3.72	4.73	5.61	6.28
0.2	1.22	1.59	1.56	1.48	1.76
0.4	1.17	1.10	1.33	1.75	1.69
0.8	0.54	0.65	0.61	0.67	1.01
1.6	0.20	0.16	0.18	0.33	0.44
3.2	0.08	0.02	0.02	0.02	0.14

decay of error in the estimation of the hidden states, dependent on $\|e^{A_d T}\|_2$ from (16), and shown in Fig. 6. Thus, the impact of hidden states on the prediction precision of data-enabled inverse operator can be reduced by using sufficient time history of the desired output.

Remark 3. (Reducing hidden state dependence). In the following simulations, the time history T is chosen to be sufficiently large $T^* = 3.2$ s, which results in a normalized error $e_u \approx 0.01\%$.

3.5 Need to include output time derivatives

From (24) in Lemma 2, even if the hidden state error is reduced by having sufficiently large time history T , (as shown in the previous subsection), current time derivatives of the output $\xi_d(t), y^{(r)}(t)$ are needed to achieve precision prediction with the inverse operator. Therefore, the impact of adding time-derivative information is investigated through the following two steps, for different sampling

periods $\Delta t \in \{0.05s, 0.1s, 0.2s\}$ and for different number N of neurons in the hidden layer.

- (i) Incrementally including higher-order time derivatives of the output when learning the inverse operator $\mathbb{G}_{d,l}^{-1}$ that predicts the inverse input \hat{u}_d similar to (37), where output time derivatives till order l ($0 \leq l \leq 4$) are included in the data-enabled operator learning, e.g., with $l = i \geq 0$,

$$\hat{u}_d[m] = \mathbb{G}_{d,i}^{-1}[y_d[m - m_T : 1 : m], y_d^{(i)}[m], y_d^{(i-1)}[m], \dots, y_d^{(0)}[m]], \quad (38)$$

where $\mathbb{G}_{d,2}^{-1} = \mathbb{G}_d^{-1}$ in (37).

- (ii) Adding the output’s time derivatives $\dot{y}_d(t), \ddot{y}_d(t)$ to NARX-type inverse operators where the inverse operator is learned using both input and output time history, i.e., to compare

$$\hat{u}_d[m] = \text{NARX}[y_d[m - m_T : 1 : m], u_d[m - m_T : 1 : m - 1]] \quad (39)$$

$$\hat{u}_d[m] = \text{NARX}^*[y_d[m - m_T : 1 : m], \dot{y}_d[m], \ddot{y}_d[m], u_d[m - m_T : 1 : m - 1]]. \quad (40)$$

The corresponding prediction performance, in terms of errors e_u and \bar{e}_u in (35), for $T^* = 3.2$ s and $\Delta t = 0.05$ s are tabulated in Table 3, and plotted in Fig 7 for $T^* = 3.2$ s and different sampling time $\Delta t \in \{0.05s, 0.1s, 0.2s\}$.

Table 3. Prediction error e_u, \bar{e}_u (35) for inverse operators from (38) to (40) with $\Delta t = 0.05$ s.

	$e_u(\%)$	$\bar{e}_u(\%)$		$e_u(\%)$	$\bar{e}_u(\%)$
Noise free training data					
$\mathbb{G}_{d,0}^{-1}$	3.13	9.82	$\mathbb{G}_{d,4}^{-1}$	0.01	0.02
$\mathbb{G}_{d,1}^{-1}$	0.74	2.10	NARX	1.60	5.93
$\mathbb{G}_{d,2}^{-1} = \mathbb{G}_d^{-1}$	0.01	0.02	NARX*	0.01	0.02
$\mathbb{G}_{d,3}^{-1}$	0.01	0.02			
Noisy training data					
$\mathbb{G}_{d,0}^{-1}$	53.91	114.68	$\mathbb{G}_{d,4}^{-1}$	0.41	0.78
$\mathbb{G}_{d,1}^{-1}$	11.53	37.82	NARX	3.89	17.95
$\mathbb{G}_{d,2}^{-1} = \mathbb{G}_d^{-1}$	0.53	1.05	NARX*	0.21	0.45
$\mathbb{G}_{d,3}^{-1}$	0.65	1.32			

Impact of including derivatives The precision of the inverse operator depends on inclusion of the output derivative upto order r (the relative degree). When the number of derivatives l (included in the training and evaluation) is increased from $l = 0$ to $l = 4$, the precision of the inverse operator improves significantly when all the required number ($l = 2 = r$) of time derivative features are included in the training and evaluation data. In particular, the maximum error \bar{e}_u in (35) reduces from 9.82% to 0.02% for the case with noise free training data and from 114.68% to 1.05% for the case with noisy training data as seen in Table 3. Therefore, there is substantial improvement in the inverse operator’s precision (especially in the presence of noise) when time derivatives upto the required order of 2 are included.

Impact on NARX-type inverse operator Inclusion of time derivatives is also important for NARX-type inverse operators where both input and output time history are used in the inverse operator. This can be seen by comparing NARX (39) without time derivatives and NARX*

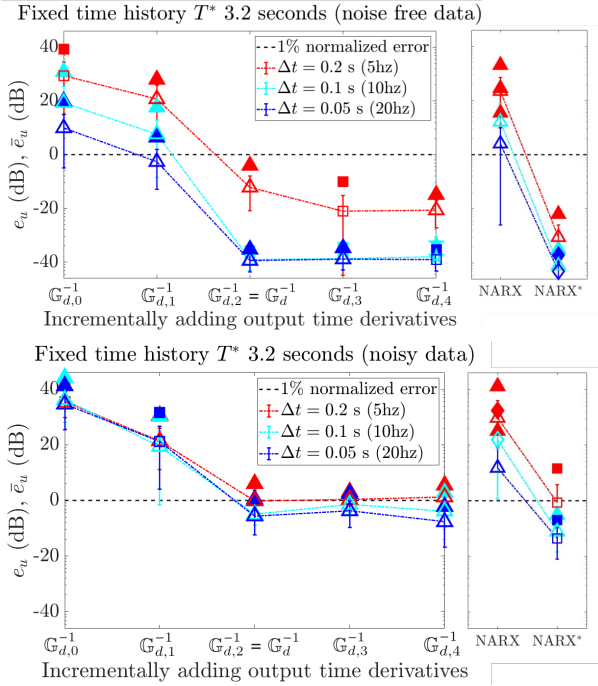


Fig. 7. Inverse operator’s precision in terms of prediction error e_u, \bar{e}_u (35) improves for all cases with the addition of derivative information. (Top: noise free training data. Bottom: noisy training data). Similar results are seen for different number N^* of neurons in the hidden layer, with symbols as in Fig. 6, where the filled symbols correspond to \bar{e}_u and unfilled correspond to e_u . Performance of NARX-type operator with input and output history but without derivative information is also improved with the addition of derivative information in NARX*, as in (39,40)

(40) with the derivatives in Table 3 and in Fig 7. When time derivatives $l = 2$ are included in the training and evaluation, the precision of the inverse operator improves significantly. In particular, the maximum error \bar{e}_u in (35) reduces from 5.93% to 0.02% for the case with noise free training data and from 17.95% to 0.45% for the case with noisy training data as seen in Table 3. Therefore, there is substantial improvement in the precision of the NARX-type inverse operator when the output time derivatives upto the required order of 2 are included.

Derivative information in output time history Conceptually, information about the derivatives upto $r - 1$ (one less than the relative degree r) are available in the time history of the output and only the r^{th} time derivative $y_d^{(r)}[m]$ is directly affected by the input $u[m]$. In particular, output derivatives can be related to the output time history using finite difference techniques, especially in the noise free case, and hence direct computation of the derivatives might not appear to be critical if time history of the output is used during training. Nevertheless, including computed or measured values (even with some noise) of the time derivative $\dot{y}[m]$ (which is not directly affected by the input $u[m]$) still can improve the precision of the inverse

operator as seen in Fig. 7 and Table 3. In particular, the maximum error \bar{e}_u in (35) reduces from 9.82% to 2.10% for the case with noise free training data and from 114.68% to 37.82% for the case with noisy training data as seen in Table 3. Therefore, while the noise free case precision could be improved by smaller sampling time Δt without the inclusion of \dot{y} , for the noisy case, direct measurements of the output time derivatives can substantially improve the inverse operator training, and lead to better precision in its predictions. Moreover, the precision of the inverse operator is further improved by including time derivatives upto the required order of r (relative degree).

4. CONCLUSION

This work showed that Koopman-type data-enabled inverse operators can have high precision if a sufficient large time history of the output is included to reduce the impact of hidden internal states. Additionally, measurements of the instantaneous output time derivatives (upto the relative degree) are required during training to improve the data-enabled inverse operator precision. Our ongoing work is aimed at extending these results to Koopman-type data-enabled inverse operators for nonlinear nonminimum-phase systems.

REFERENCES

- Aarnoudse, L., Ohnishi, W., Poot, M., Tacx, P., Strijbosch, N., and Oomen, T. (2021). Control-relevant neural networks for intelligent motion feedforward. In *2021 IEEE International Conference on Mechatronics (ICM)*, 1–6. IEEE.
- Abraham, I., De La Torre, G., and Murphey, T.D. (2017). Model-based control using koopman operators. In *2017 Robotics: Science and Systems, RSS 2017*. MIT Press Journals.
- Asadi, F., Olleak, A., Yi, J., and Guo, Y. (2021). Gaussian process (GP)-based learning control of selective laser melting process. In *2021 American Control Conference (ACC)*, 508–513. IEEE.
- Blanken, L. and Oomen, T. (2020). Kernel-based identification of non-causal systems with application to inverse model control. *Automatica*, 114, 108830.
- Brunton, S.L., Proctor, J.L., and Kutz, J.N. (2016). Discovering governing equations from data by sparse identification of nonlinear dynamical systems. *Proceedings of the national academy of sciences*, 113(15), 3932–3937.
- Butterworth, J.A., Pao, L.Y., and Abramovitch, D.Y. (2012). Analysis and comparison of three discrete-time feedforward model-inverse control techniques for nonminimum-phase systems. *Mechatronics*, 22(5), 577–587.
- Desoer, C.A. and Vidyasagar, M. (1975). *Feedback Systems: Input-output Properties*, volume 55. SIAM.
- Devasia, S., Chen, D., and Paden, B. (1996). Nonlinear inversion-based output tracking. *IEEE Transactions on Automatic Control*, 41(7), 930–943.
- Devasia, S. (2017). Iterative machine learning for output tracking. *IEEE Transactions on Control Systems Technology*, 27(2), 516–526.
- Fine, B.T., Mishra, S., and Tomizuka, M. (2009). Model inverse based iterative learning control using finite impulse response approximations. In *2009 American Control Conference*, 931–936. IEEE.

- Ghosh, J. and Paden, B. (2001). Iterative learning control for nonlinear nonminimum phase plants. *J. Dyn. Sys., Meas., Control*, 123(1), 21–30.
- Hewing, L., Wabersich, K.P., Menner, M., and Zeilinger, M.N. (2020). Learning-based model predictive control: Toward safe learning in control. *Annual Review of Control, Robotics, and Autonomous Systems*, 3, 269–296.
- Kabzan, J., Hewing, L., Liniger, A., and Zeilinger, M.N. (2019). Learning-based model predictive control for autonomous racing. *IEEE Robotics and Automation Letters*, 4(4), 3363–3370.
- Kamb, M., Kaiser, E., Brunton, S.L., and Kutz, J.N. (2020). Time-delay observables for koopman: Theory and applications. *SIAM Journal on Applied Dynamical Systems*, 19(2), 886–917.
- Kocijan, J., Murray-Smith, R., Rasmussen, C.E., and Girard, A. (2004). Gaussian process model based predictive control. In *Proceedings of the 2004 American control conference*, volume 3, 2214–2219. IEEE.
- Kutz, J.N., Brunton, S.L., Brunton, B.W., and Proctor, J.L. (2016). *Dynamic mode decomposition: data-driven modeling of complex systems*. SIAM.
- Ljung, L. et al. (1987). Theory for the user. *System Identification*.
- Mamakoukas, G., Castano, M.L., Tan, X., and Murphey, T.D. (2021). Derivative-based koopman operators for real-time control of robotic systems. *IEEE Transactions on Robotics*.
- Marino, R. and Tomei, P. (1995). *Nonlinear control design*. Prentice-Hall International.
- Mezić, I. (2005). Spectral properties of dynamical systems, model reduction and decompositions. *Nonlinear Dynamics*, 41(1), 309–325.
- Pham, H.T., Yang, B.S., et al. (2010). A hybrid of nonlinear autoregressive model with exogenous input and autoregressive moving average model for long-term machine state forecasting. *Expert Systems with Applications*, 37(4), 3310–3317.
- Piche, S., Keeler, J.D., Martin, G., Boe, G., Johnson, D., and Gerules, M. (2000). Neural network based model predictive control. In *Advances in Neural Information Processing Systems*, 1029–1035.
- Pohle, J., Langrock, R., van Beest, F.M., and Schmidt, N.M. (2017). Selecting the number of states in hidden markov models: pragmatic solutions illustrated using animal movement. *Journal of Agricultural, Biological and Environmental Statistics*, 22(3), 270–293.
- Schmid, P. and Sesterhenn, J. (2008). Dynamic mode decomposition of numerical and experimental data. *Bulletin of the American Physical Society*, 53.
- Spiegel, I.A., Strijbosch, N., Oomen, T., and Barton, K. (2021). Iterative learning control with discrete-time nonlinear nonminimum phase models via stable inversion. *International Journal of Robust and Nonlinear Control*, 31(16), 7985–8006.
- Tarbouriech, J., Shekhar, S., Pirotta, M., Ghavamzadeh, M., and Lazaric, A. (2020). Active model estimation in markov decision processes. In *Conference on Uncertainty in Artificial Intelligence*, 1019–1028. PMLR.
- Teng, K.T. and Tsao, T.C. (2015). A comparison of inversion based iterative learning control algorithms. In *2015 American Control Conference (ACC)*, 3564–3569. IEEE.
- Willems, J.C., Rapisarda, P., Markovskiy, I., and De Moor, B.L. (2005). A note on persistency of excitation. *Systems & Control Letters*, 54(4), 325–329.
- Yan, L.L., Banka, N., Owan, P., Piaskowy, W.T., Garbini, J.L., and Devasia, S. (2021). MIMO ILC using complex-kernel regression and application to precision sea robots. *Automatica*, 127, 109550.
- Yoon, H.J., Lee, D., and Hovakimyan, N. (2019). Hidden markov model estimation-based Q-learning for partially observable markov decision process. In *2019 American Control Conference (ACC)*, 2366–2371. IEEE.
- Zou, Q. and Devasia, S. (1999). Preview-based stable-inversion for output tracking of linear systems. *ASME J. Dyn. Syst. Meas. Control*.
- Zou, Q. and Devasia, S. (2007). Precision preview-based stable-inversion for nonlinear nonminimum-phase systems: The vtol example. *Automatica*, 43(1), 117–127.

Appendix A. EVALUATION TRAJECTORIES

Expressions of $y_{0,k}(t)$ for $k = 1, 2, \dots, 10$ and $0 \leq t \leq 10$. Trapezoidal shape ($k = 1$)

$$y_{0,1}(t) = \begin{cases} 0.4(t-1) & 1 \leq t < 3 \\ 0.8 & 3 \leq t < 6 \\ 0.4(8-t) & 6 \leq t < 8 \\ 0 & \text{otherwise.} \end{cases}$$

Triangle wave ($k = 2$)

$$y_{0,2}(t) = \begin{cases} t-2 & 2 \leq t < 3 \\ 3.7-0.9t & 3 \leq t < 5 \\ t-5.8 & 5 \leq t < 7 \\ 1.2(8-t) & 7 \leq t < 8 \\ 0 & \text{otherwise.} \end{cases}$$

Square wave ($k = 3$)

$$y_{0,3}(t) = \begin{cases} 1 & 2 \leq t < 4 \\ -1 & 4 \leq t < 6 \\ 1 & 6 \leq t < 8 \\ 0 & \text{otherwise.} \end{cases}$$

Serrated wave mixture ($k = 4$)

$$y_{0,4}(t) = \begin{cases} 2(t-1)/3 & 1 \leq t < 2.5 \\ 2(4-t)/3 & 2.5 \leq t < 4 \\ 8(t-4)/15 & 4 \leq t < 5 \\ 8(6-t)/15 & 5 \leq t < 6 \\ 0.4(t-6) & 6 \leq t < 7.5 \\ 0.4(9-t) & 7.5 \leq t < 9 \\ 0 & \text{otherwise.} \end{cases}$$

Monotonic ($k = 5$): $y_{0,5}(t) = 0.001(x^{3.2} - x^2)$ Sine wave #1 ($k = 6$)

$$y_{0,6}(t) = \sin(0.4\pi t) - 0.9\sin(0.6\pi t) + 0.2\sin(\pi t)$$

Sine wave #2 ($k = 7$)

$$y_{0,7}(t) = 1.5\sin(0.7\pi t) - 0.5\sin(0.4\pi t)$$

Sine wave #3 ($k = 8$)

$$y_{0,8}(t) = -0.5\sin(0.3\pi t) - 0.6\sin(0.7\pi t) + 0.2\sin(1.2\pi t)$$

Sine wave #4 ($k = 9$)

$$y_{0,9}(t) = 0.7\sin(0.26\pi t) + 0.3\sin(1.3\pi t) - 0.2\sin(1.4\pi t)$$

Slow chirp wave ($k = 10$): $y_{0,10}(t) = 0.35\sin(x^{1.5})$.